Classification
Physics Abstracts
61.16Bg — 68.55Nq — 74.76Bz — 81.15Cd

Inclusions in Magnetron Sputtered $YBa_2Cu_{3-x}M_xO_{7-\delta}$ Thin Films: A Study by Means of Electron Microscopy

Karen Verbist([1]), Gustaaf Van Tendeloo([1]), Min Ye([2]), Jeannot Schroeder([2]), Mohammad Mehbod([2]) and Robert Deltour([2])

([1]) EMAT, University of Antwerp (R.U.C.A.), Groenenborgerlaan 171, 2020 Antwerpen, Belgium
([2]) Physique des Solides, CP-233, Université Libre de Bruxelles, Boulevard du triomphe, 1050 Bruxelles, Belgium

(Received November 25, accepted December 15, 1995)

Abstract. — The microstructure of (001) $YBa_2Cu_3O_{7-\delta}$ and $YBa_2Cu_{3-x}M_xO_{7-\delta}$ (M = Zn or Fe) thin films grown by inverted cylindrical magnetron sputtering was investigated by means of electron microscopy. The imperfections present in the films are discussed. Special attention is paid to nanoscale Y_2O_3 inclusions. The density of [001] Y_2O_3 precipitates was studied in $YBa_2Cu_{3-x}Zn_xO_{7-\delta}$ and $YBa_2Cu_{3-x}Fe_xO_{7-\delta}$ thin films prepared under identical conditions. The density decreases for increasing Zn-content and is unaffected in case of Fe-substitution.

1. Introduction

Soon after the discovery of the bulk $YBa_2Cu_3O_{7-\delta}$ (123) compound thin films were produced by various deposition techniques (see e.g. [1]). Now 123 films are prepared on a routine basis by *in-situ* processes from a single target which yields epitaxial thin films with T_c values of 91 K and J_c values in the vicinity of 10^7 A/cm^2 [2]. A film growth process optimised to yield high T_c and J_c values does not necessarily yield perfect materials from the structural point of view. The segregation of secondary phase outgrowths is very common and difficult to solve when one is constrained by other optimisation parameters such as electrical properties.

The characterization of the microstructure by a number of techniques including analytical electron microscopy (AEM) and high resolution electron microscopy (HREM) is essential for the understanding of the behaviour of the materials e.g. [3, 4]. Electron microscopy techniques provide detailed information on crystal defects such as stacking faults, secondary phase inclusions, dislocations, grain boundaries or twins. Moreover HREM-images from film cross-sections also provide atomic scale information on the film substrate interface. Because of its high resolving power and the ability to focus the beam down to nanoscale, electron microscopy in general is particularly suited to study the occurrence of small nanometer size secondary phase precipitates in thin films.

In the present work we have characterized by means of electron microscopy (HREM and AEM), the defects/imperfections present in (001) 123 thin films and investigated the effect of Zn-substitution or Fe-substitution on the Y_2O_3 inclusion density in these films. All films were deposited by inverted cylindrical magnetron sputtering on single crystal (100) $SrTiO_3$ or (100) MgO.

2. Experimental

Pure, Zn and Fe-doped epitaxial $YBa_2Cu_3O_{7-\delta}$ thin films were grown *in situ* on single crystal (100) $SrTiO_3$ and (100) MgO substrates using inverted cylindrical magnetron sputtering. The optimisation of the deposition technique was reported elsewhere [5]. Briefly, the deposition parameters involved are: substrate temperature of 780 °C, O_2 partial pressure of 0.3 mbar, total Ar + O_2 pressure around 0.6 mbar, sputtering power 60 W and a deposition rate of 7.5 nm/min. After deposition, the films were oxygenated at 450 °C for 25 min. The substitution was introduced by sputtering under the same conditions from a stoichiometric bulk $YBa_2Cu_{3-x}M_xO_{7-\delta}$ target with M = Zn or Fe and $x = 0, 0.06, 0.12$ or 0.18. We will in the following refer to the 123 films with 2%, 4% and 6% Zn as Zn2, Zn4 and Zn6 respectively and to the 4% Fe film as Fe4.

For the electron diffraction study a Philips CM20 microscope equipped with a LINK 2000 QX energy dispersive X-ray analyser (EDX) was used. The high resolution (HREM) work was carried out on a JEOL 4000 EX microscope operating at 400 keV with a point resolution of 0.17 nm. Plan view TEM samples were polished down to 30 μm before backside ion thinning. Cross-section samples were prepared in the conventional way.

3. Results and Discussion

3.1 PHYSICAL PROPERTIES. — AC susceptibility measurements, performed in the configuration with AC magnetic fields aligned perpendicular to the film surface, show onset transition temperatures of 87, 76, 66 and 52 K with a transition width of 1, 2, 3 and 5 K for pure, Zn2, Zn4 and Zn6 respectively. The measured T_c values for the 123 thin films with Zn allow an estimate of the substitution level in the films, found in Table I, by comparison with doped bulk compounds [6] and thin films [7]. This estimate together with the uncertainty of the EDX composition analysis leads to the conclusion that the actual Zn-substitution content is somewhat lower then the nominal one in the targets. This can be understood when taking into account the high volatility of Zn. The T_c of Fe4, measured the same way is 78 K. The actual substitution level therefore approximates the nominal one.

Figure 1 shows the J_c values in zero field for pure 123 films on $SrTiO_3$ (A) and MgO (B) measured indirectly by AC susceptibility measurements before patterning and direct on a patterned micro bridge. Clearly the pure films have J_c values around 10^7 A/cm^2 at 77 K in zero field [5]. By applying the Bean-model [8] to the AC susceptibility measurements, J_c values in the vicinity of T_c were determined and listed in Table I. X-ray diffraction patterns ($\theta - 2\theta$ scans) of the films indicate that all films are oriented with the c-axis perpendicular to the substrate surface. Further study of the epitaxy by rocking curves taken from the (005) lines reveals mosaic spreads of 0.2, 0.33, 0.45, and 1.10° for the pure and Zn-doped films deposited from $YBa_2(Cu_{1-x}Zn_x)_3O_{7-\delta}$ targets with $x = 0, 0.02, 0.04$, and 0.06, respectively (Tab. I). Clearly the quality of the epitaxy decreases with increasing Zn-substitution.

3.2 STRUCTURAL PROPERTIES. — TEM investigations revealed that the pure 123 thin films on (100) $SrTiO_3$ are of high quality with a good epitaxy and almost free of large impurity phases. The films are orthorhombic with a high density of twin boundaries roughly spaced by 40 to 50 nm.

Table I. — *Superconducting and structural properties of pure and* Zn-*doped epitaxial* $YBa_2Cu_3O_{7-\delta}$ *thin films.*

Sample	pure	2% Zn	4% Zn	4% Fe	6% Zn
T_c,on(K)[a]	87	76	66	78	52
ΔT_c (K)[a]	1	2	3	4	5
M-content[b] (%)	0	1.6	2.6	4.5	4
J_c at T/T_c =0.9 (10^6A/cm^2)[c]	9.5	1.3	0.56	0.1	0.14
Mosaic spread(°)[d]	0.2	0.33	0.45	--	1.1
# $[001]_{Y2O3}$ (10^{16}/cm^3)[e]	11±2	10±2	2.5±2	14±2	/

[a]AC susceptibility measurements.

[b]Estimated from T_c values.

[c]J_c values determined from the transport measurements (for pure films) and from the AC susceptibility measurements using the Bean-model (for the Zn and Fe-films)

[d]From rocking curves of the (005) lines

[e] numerical density estimated from plan view and cross-section TEM-micrographs

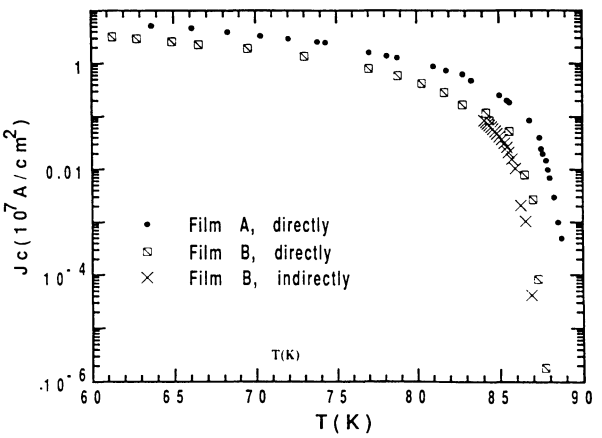

Fig. 1. — The critical current densities for pure 123 films on $SrTiO_3$ (A) and MgO (B) measured indirectly and directly in zero field.

The size of the domains with parallel twin boundaries is approximately 1 μm as can be seen from the plan view section (Fig. 2). At higher magnifications some small precipitates can be observed (see inset of Fig. 2). From HREM (Fig. 3) and optical diffraction they are identified as Y_2O_3 inclusions, previously also reported by Eibl *et al.* [4], Catana *et al.* [9] and others. These inclusions with sizes between 100 and 1000 nm^3 grow with the following orientation relationship: with respect to the surrounding 123:

$$[100]_{Y_2O_3} //[110]_{123}, [010]_{Y_2O_3} //[1\bar{1}0]_{123}, [001]_{Y_2O_3} //[001]_{123}.$$

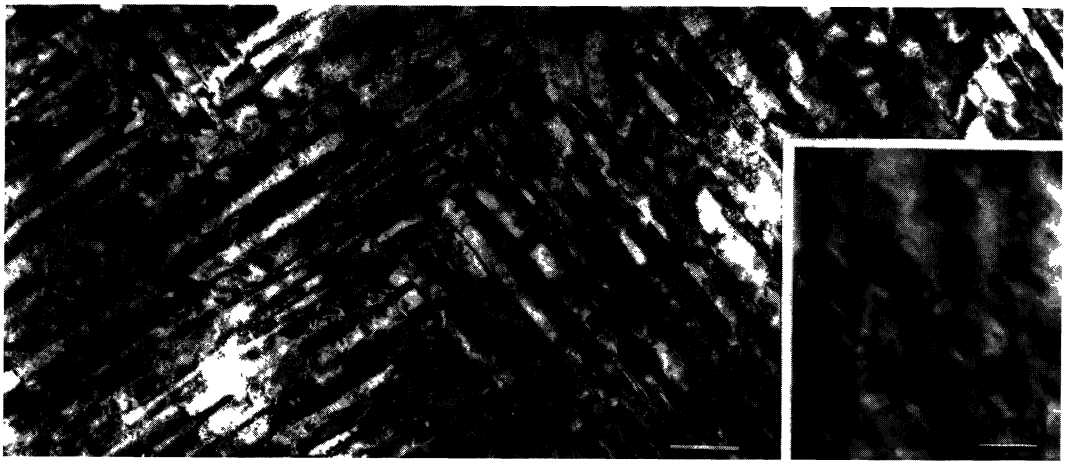

Fig. 2. — Plan-view TEM-micrograph showing {110}-twin boundaries in the pure 123 film on $SrTiO_3$. The inset shows square precipitates, superimposed on the twin boundary pattern, identified as Y_2O_3 inclusions.

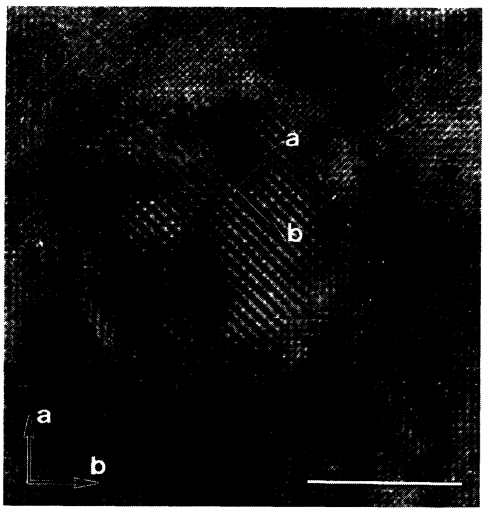

Fig. 3. — HREM-micrograph showing a Y_2O_3 inclusion with the [100]-axis parallel to the [110]-axis of 123.

Optical diffraction of the precipitates and the presence of Moiré-fringes indicate they are sometimes slightly misaligned with respect to the c_{123}-axis. The density of these [001] Y_2O_3 precipitates as calculated with an estimated sample thickness of 10 nm from plan-view and cross-sectional micrographs is $1.1 \times 10^{17}/cm^3$ (see Tab. I). Combined plan view images and cross-section images such as Figure 4, provide evidence that the precipitates have roughly the same dimensions in the ab_{123}-plane as along the c_{123}-axis. The cube form we report here is different from the disk-like shape reported by Dorignac *et al.* [10] and Lu *et al.* [11]. We did find some platelet-like precipitates such as reported by [10, 11], but they were a minority.

The thin films apparently also contain another type of nanosize inclusion. The high resolution micrograph of Figure 5 shows a rectangular precipitate with an average width of 5 nm and

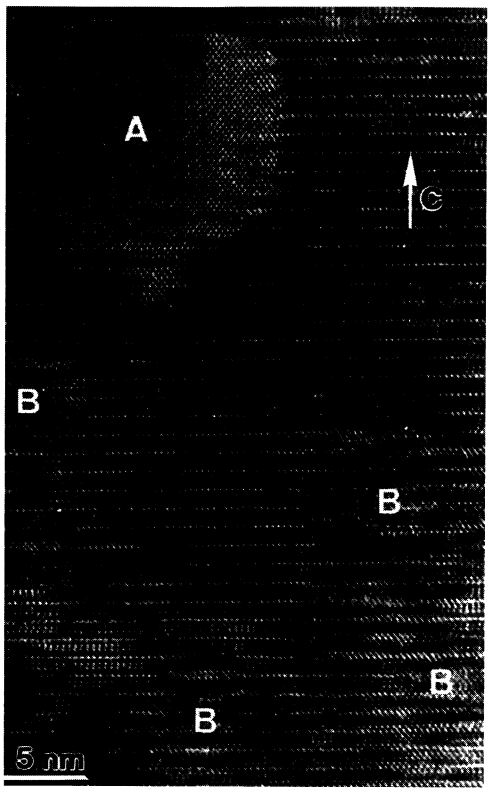

Fig. 4. — Cross-section TEM micrograph of the Zn2 film. Y_2O_3 inclusions are marked by A (no overlap) and B (overlap with 123). The Y_2O_3 inclusions are cuboids.

a length scale which is typically the double of the width. The exact composition is hard to determine because of the small dimensions. The diffractogram together with image calculations however indicate that this precipitate is also Y_2O_3 [12] but in a different orientation with respect to the surrounding 123, namely:

$$[1\bar{1}0]_{Y_2O_3} //[100]_{123}, [110]_{Y_2O_3} //[001]_{123}, [001]_{Y_2O_3} //[010]_{123}.$$

This type of precipitate however occurs only at the surface of the thin films. The surface density for this type of [110] Y_2O_3 precipitates is much lower than that for the cube-like [001] Y_2O_3 precipitates and was calculated to be $7 \times 10^9/cm^2$.

EDX identified surface outgrowths occurring in all samples, to be copper oxide particles with an average diameter of nearly 1 μm. Although X-ray diffraction indicated the films to be c-axis oriented, a very small fraction of the films consists of grains with their c-axis in a plane parallel to the interface, so-called a-axis grains. On the film surface they have a characteristic needle like shape and are connected to secondary phase grains such as $Y_2Ba_1Cu_1O_5$ or Y_2O_3 [9]. A commonly observed and well characterized defect in 123 are the CuO (001) double layers. They are numerously present although they do not occur periodically to form the 124 phase but are randomly distributed in the film.

When viewing along the 123 [001] direction translational type defects situated in the (100) or (010) planes have been observed (Fig. 6a). Across both interfaces, a lattice shift is observed and

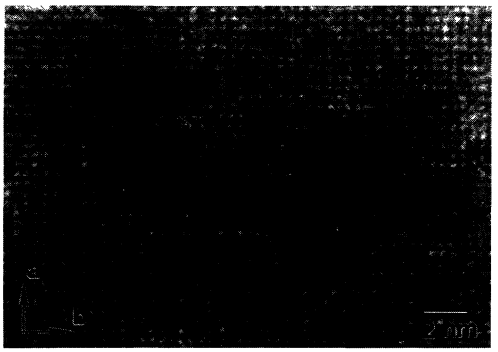

Fig. 5. — HREM along $[001]_{123}$ of a $[110]_{Y_2O_3}$ inclusion in a pure 123 film.

a displacement vector of the type $R = \left[\frac{1}{2}\frac{1}{2}\, w\right]$ can be associated with both stacking defects. These defects form closed tubes along the [001] viewing direction. Eibl *et al.* [4] have observed similar defects and termed them "stacking fault cuboids"; although we do not find evidence for a closed cage along the (001) planes. Anyway, translational defects of the type $\left[\frac{1}{2}\frac{1}{2}\, w\right]$, situated in (001) or (010) planes necessarily alter the local composition and can therefore be denoted as non-conservative antiphase boundaries. Let us consider the situation of the defect located along the (100) plane (Fig. 6b). In the orthorhombic 123, the (100) layers are alternating $Cu_3O_{3-\delta}$ and YBa_2O_4; therefore any translation interface with a displacement vector $R = \left[\frac{1}{2}\frac{1}{2}\, w\right]$ will introduce a double layer of $Cu_3O_{3-\delta}$ or a double layer of YBa_2O_4. As a consequence the local composition will be altered and will be copper rich or copper deficient. In view of the fact that extra Cu-O can be incorporated into the 123-YBCO structure [13] it is most probable that the present defects are Cu-rich, and have the configuration as represented in Figure 6b.

The EDX analysis performed in SEM and TEM over a large film area or averaged over different probe positions indicates deviations from the ideal 123 stoichiometry. The films are rich in yttrium and slightly rich in copper although the targets were stoichiometric and the sputtering process was optimised. This off-stoichiometry is obviously compensated by the formation of Y_2O_3 precipitates and CuO surface outgrowths and Cu-rich defects such as stacking fault cuboids and CuO double layers. Nevertheless such non-stoichiometric films may have good transport properties as is demonstrated here and reported in the works of Sidorov *et al.* [3] and Matijasevic *et al.* [14], all for Ba-deficient 123 films.

SEM analysis indicated that the surface morphology of the films changes with an increasing substitution level from 0 to 6% Zn although the films were deposited under the same conditions. The surface of the Zn2 film is smooth with limited outgrowths while the surface of the Zn4 film contains pinholes. Chew *et al.* [15] found this morphology characteristic for Cu-deficient thin films. Low magnification plan view TEM and EDX were used to characterize inclusions found in the SEM-micrographs. Cross-section TEM was used to study possible changes in the bulk of the films. The occurrence of second phase inclusions in a micron size range results from the non-stoichiometry of the 123 films. EDX-analysis showed the average composition to be Y-rich and slightly Cu-rich also for the substituted films although the targets were stoichiometric and the sputtering process was the same as for the pure 123 films. No regions with higher Zn- or Fe-concentration than the average M-content in the film could be detected by EDX.

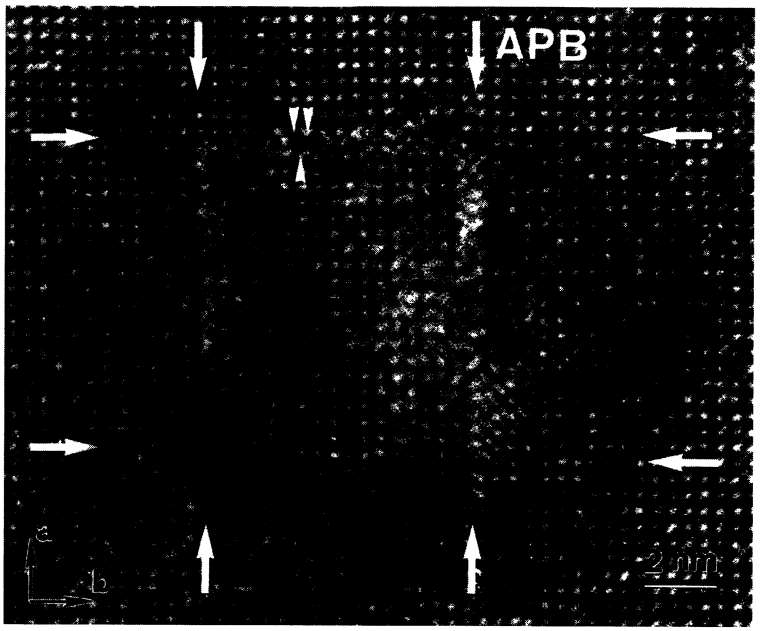

a)

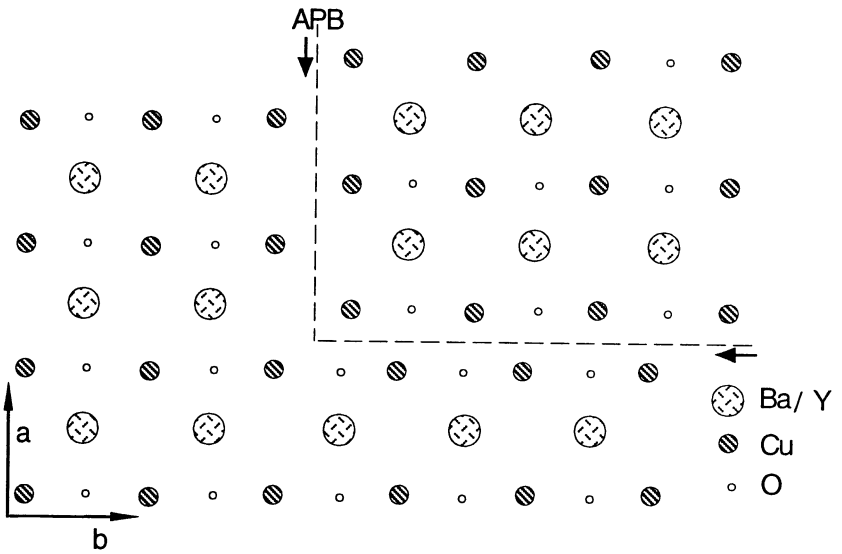

b)

Fig. 6. — a) HREM view along the 123 [001]-direction showing non-conservative antiphase boundaries situated along (001) or (010) planes with a displacement vector of the type $R = \left[\frac{1}{2}\frac{1}{2}w\right]$; b) schematic drawing of the defect configuration assuming that the defects are Cu-rich.

The microstructure of the Zn6 sample consists of c-axis oriented 123 blocks with an average side of 0.4 μm separated from each other by secondary phases and voids. These phases have been identified by SAED and EDX to be a-axis 123 grains, 211, Y_2O_3, ... The characteristic signs of

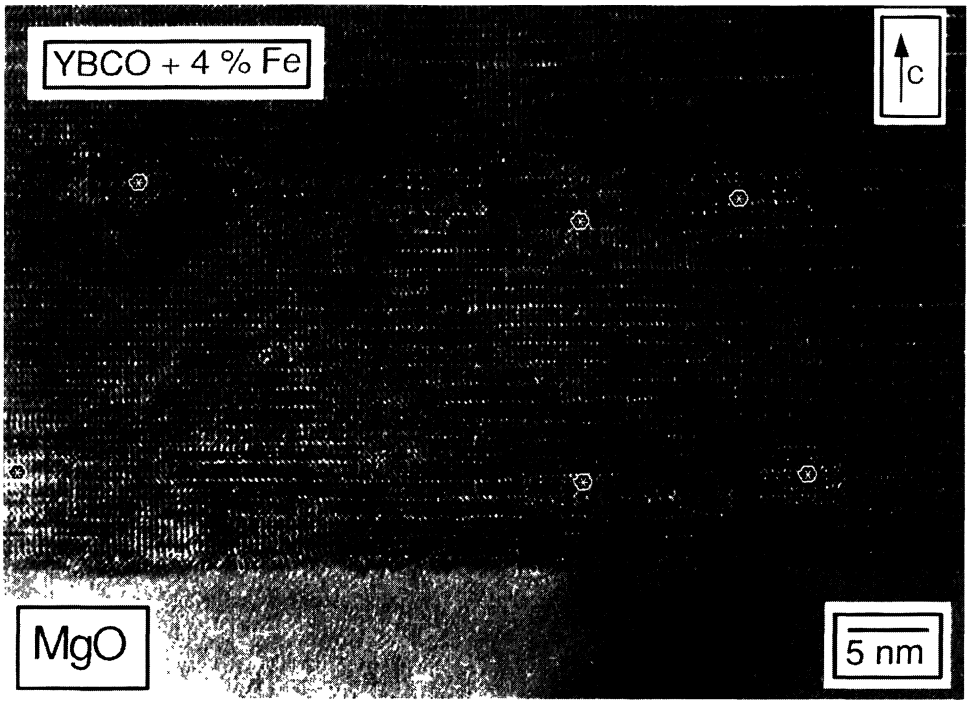

Fig. 7. — Cross-section TEM micrograph of the Fe4 film. The Y_2O_3 precipitates (marked by an asterisk) are more disk shaped.

orthorhombicity, namely the presence of twin boundaries in the direct image and spot splitting in the diffraction pattern are no longer present in the Zn6 sample although clearly present in the Zn2 and Zn4 sample. Therefore we conclude that the orthorhombicity is severely decreased if not totally absent for the film with 6% Zn. This film was omitted when investigating the presence of precipitates. Apparently the optimised deposition conditions for pure 123 are no longer valid in this case.

Thin films with 4% of copper substituted by iron (Fe4) have the same microstructural features as the pure 123 films which were investigated. The density of [001] Y_2O_3 precipitates is $1.4 \times 10^{16}/cm^3$, a value comparable with the pure 123 and Zn2 films. The shape of the precipitates is more disklike as can be seen in Figure 7.

When analysing the density of [001] Y_2O_3 precipitates as a function of the Zn-substitution level (Tab. I) we find that the density remains nearly constant for a 2% Zn substitution. The density decreases considerably if the substitution is further increased to 4%. Ways to influence the Y_2O_3 precipitates density have been discussed such as adding a fraction of N_2O in the sputtering gas [16]. Here the influencing factor is the Zn-substitution level. However the mechanisms behind this are not clear. The amount of Cu (and Cu- replacing element) is affected because of the high volatility of Zn. This together with film composition (slight excess of Cu and excess of Y) should cause a larger Y excess which could lead to more Y_2O_3 precipitates. This is not the case. The excess Y can also be incorporated as other secondary phases such as $Y_2Ba_1Cu_1O_5$ or $Y_2Cu_2O_5$. The density of large micron size outgrowths is not increased when comparing the Zn2 and Zn4 films. However the formation process of Zn-substituted thin films is also affected in another way since

a SEM study showed that the optimum deposition conditions yielding smooth pure YBCO films is not the best condition for growing smooth Zn-substituted films.

4. Conclusion

An inventory of structural imperfections in magnetron sputtered films with good physical properties was made. Most prominent feature of these Ba-deficient films is the high density of Y_2O_3 precipitates which occur in two different orientations. The density of Y_2O_3 [001] precipitates decreases considerably when nominally 4% of Zn is substituted but remains unchanged for 2% Zn-substitution or 4% Fe-substitution.

Acknowledgements

The authors would like to thank L. Rossou and G. Stoffelen for the TEM specimen preparation and A.L. Vasiliev for fruitful discussions. This research has been supported by the Belgium National Program on high T_c superconductivity (SU/03/17 for K.V. and SU/02/09 for M.Y.)

References

[1] Kautek W., *Vacuum* **43** (1992) 403.

[2] Scheel H.J., Berkowski M. and Chabot B., *J. Crystal Growth* **115** (1991) 19.

[3] Sidorov M.V., Oktyabrsky S. and Krasnosvobodtsev S.I., *Mat. Sci. Eng.* **B18** (1993) 295.

[4] Eibl O. and Roas B., *J. Mater. Res.* **5** (1990) 2620.

[5] Ye M., Mehbod M. and Deltour R., *Physica B* **204** (1995) 200.

[6] Mehbod M., Biberacher W., Jansen A.G.M., Wyder P., Deltour R. and Duvigneaud P.H., *Phys. Rev. B* **38** (1988) 11813 .

[7] Tomé-Rosa C., Jacob G., Paulson M., Wagner P., Walkenhorst A., Schmitt M. and Adrian H., *Phys C* **185-189** (1991) 2175.

[8] Bean C.P., *Phys. Rev. Lett.* **8** (1962) 250 .

[9] Catana A., Broom R.F., Bednorz J.G., Mannhart J. and Schlom D.G., *Appl. Phys. Lett.* **60** (1992) 1016.

[10] Dorignac D., Schamm S., Grigis C., Sévely J., Santiso J. and Figueras A., *Phys C* **235-240** (1994) 617.

[11] Lu P., Li Q., Zhao J., Chern C.S., Gallois B., Noris P., Kear B. and Cosandey F., *Appl. Phys. Lett.* **60** (1992) 1265.

[12] Verbist K., Vasiliev A.L. and Van Tendeloo G., *Appl. Phys. Lett.* **66** (1995) 1424.

[13] Zandbergen H.W., Gronsky R. and Thomas G., *Phys. Stat. Sol. A* **105** (1988) 207.

[14] Matijasevic V., Rosenthal P., Shinohara K., Marshall A.F., Hammond R.H. and Beasley M.R., *J. Mater. Res.* **6** (1991) 682.

[15] Chew N.G., Goodyear S.W., Edwards J.A., Satchell J.S., Blenkinsop S.E. and Humphreys R.G., *Appl. Phys. Lett.* **57** (1990) 2016.

[16] Selinder T.I., Helmersson U. and Han Z., *Thin Solid Films* **229** (1993) 273.